Biophysical Journal, Volume *115*

Supplemental Information

Mechanical Mapping of Spinal Cord Growth and Repair in Living Zebrafish Larvae by Brillouin Imaging

Raimund Schlüßler, Stephanie Möllmert, Shada Abuhattum, Gheorghe Cojoc, Paul Müller, Kyoohyun Kim, Conrad Möckel, Conrad Zimmermann, Jürgen Czarske, and Jochen Guck

Supplementary Material

Mechanical mapping of spinal cord development and repair in living zebrafish larvae using Brillouin microscopy

Raimund Schlüßler[1,*,+], Stephanie Möllmert[1,+], Shada Abuhattum[1,2], Gheorghe Cojoc[1], Paul Müller[1], Kyoohyun Kim[1], Conrad Möckel[1], Conrad Zimmermann[1], Jürgen Czarske[3], and Jochen Guck[1,**]

[1]Biotechnology Center, Center for Molecular and Cellular Bioengineering, Technische Universität Dresden, Dresden, Germany
[2]JPK Instruments AG, Colditzstraße 34-36, Berlin 12099, Germany
[3]Laboratory of Measurement and Sensor System Technique, Technische Universität Dresden, Dresden, Germany
[*]Correspondence: raimund.schluessler@tu-dresden.de
[**]Correspondence: jochen.guck@tu-dresden.de
[+]these authors contributed equally to this work

SUPPLEMENTARY MATERIAL

Supplementary Note 1: Influence of reflection and absorption on the Brillouin spectrum

Measuring the Brillouin shift of a sample requires the Brillouin peaks to be clearly visible in the spectrum. This means that the signal to noise ratio (SNR) between the Brillouin peak intensity and the background noise has to be above a certain threshold. In practice, two effects can lead to a low SNR. In comparison to a clean spectrum shown in Supplementary Fig. 1a, strong reflections at refractive index gradients increase the background noise (Supplementary Fig. 1b) and high absorption due to pigments decreases the signal intensity (Supplementary Fig. 1c). In both cases, the Brillouin shift cannot be evaluated. In all Brillouin images we show such measurement points as white spots.

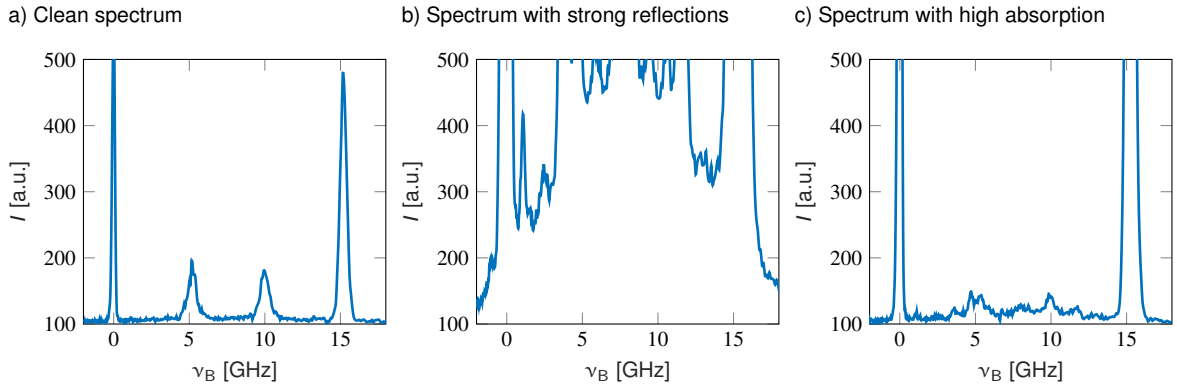

Supplementary Figure 1: Examples of Brillouin spectra for different positions inside the specimen. a) Clean spectrum with the Brillouin peaks clearly visible at 5.2 GHz and 10 GHz. Two spectra which cannot be evaluated because of b) strong reflections due to refractive index gradients and c) strong absorption of the incident light (and slightly increased reflections) due to pigments within the sample. Spectra which cannot be evaluated are discarded and shown as white spots in all Brillouin images.

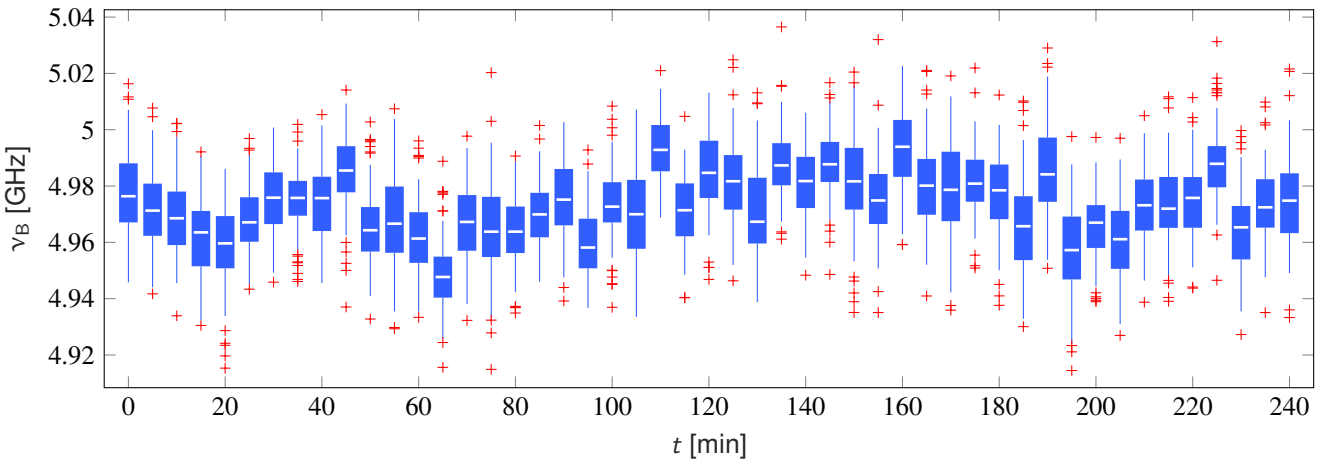

Supplementary Figure 2: Reference measurements of a water sample every 5 min over 240 min. For every time point 100 spectra were acquired with an acquisition time of 500 ms each. The mean random error amounts to 14 MHz. The maximum systematic error between the two most extreme mean values is 44 MHz, the standard deviation of the mean values is 10 MHz. The boxes indicate the interquartile ranges, the whiskers extend to the most extreme data still within 1.5 IQR of the respective quartile (Tukey boxplot) and the medians are depicted as white lines. Outliers are indicated as red crosses.

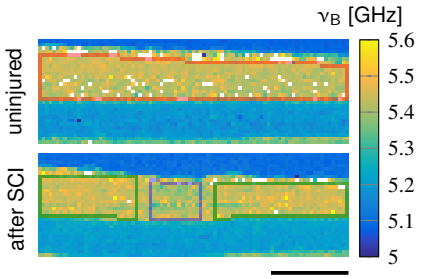

Supplementary Figure 3: The selected region of interest in the uninjured zebrafish ($N = 6$) comprises the complete spinal cord tissues (red box). For lesioned zebrafish ($N = 6$), the spinal cord tissue was divided into a region containing the lesion site (blue box) and a region for the remaining tissue (green box). Scale bar, 150 µm.

Supplementary Note 2: Comparison BM and AFM for spinal cord tissue

In order to probe the mechanical properties of muscle tissue and spinal cord tissue with an already established method, we performed AFM-based indentation measurements on acute tissue slices of larval zebrafish. The indentation setup was equipped with an upright stereo microscope which allowed to identify the respective types of tissue and target those with the cantilever tip (Supplementary Fig. 5a). The data showed that muscle tissue displayed greater apparent Young's moduli than spinal cord tissue (Supplementary Fig. 5b), which confirmed the relative mechanical difference obtained by Brillouin measurements (Fig. 7). The indentation data furthermore correlates with the longitudinal moduli calculated from refractive index and Brillouin shift measurements (Supplementary Fig. 5c).

Supplementary Note 3: Comparison of zebrafish larvae *post-mortem* and after fixation

To investigate the time dependency of the muscle stiffening *post-mortem*, we performed Brillouin microscopy on dead, but not sectioned, zebrafish larvae. The animals were mounted on their side as described for *in vivo* measurements. Their death was ensured by an overdose of MS222 and the mechanical disruption of the heart. The scanning process commenced from different starting points and followed opposite directions, i.e. from bottom to top (Supplementary Fig. 6a) and from top to bottom (Supplementary Fig. 6b) as indicated by arrows. Thereby, we were able to capture a time-dependent change of muscle tissue *post-mortem*, which showed that this type of tissue, under the conditions used here, stiffened in a time interval of approximately 1 h (scanning time for an entire map was 2 h). The measurement of the same fish twice in a row or of different fish at later

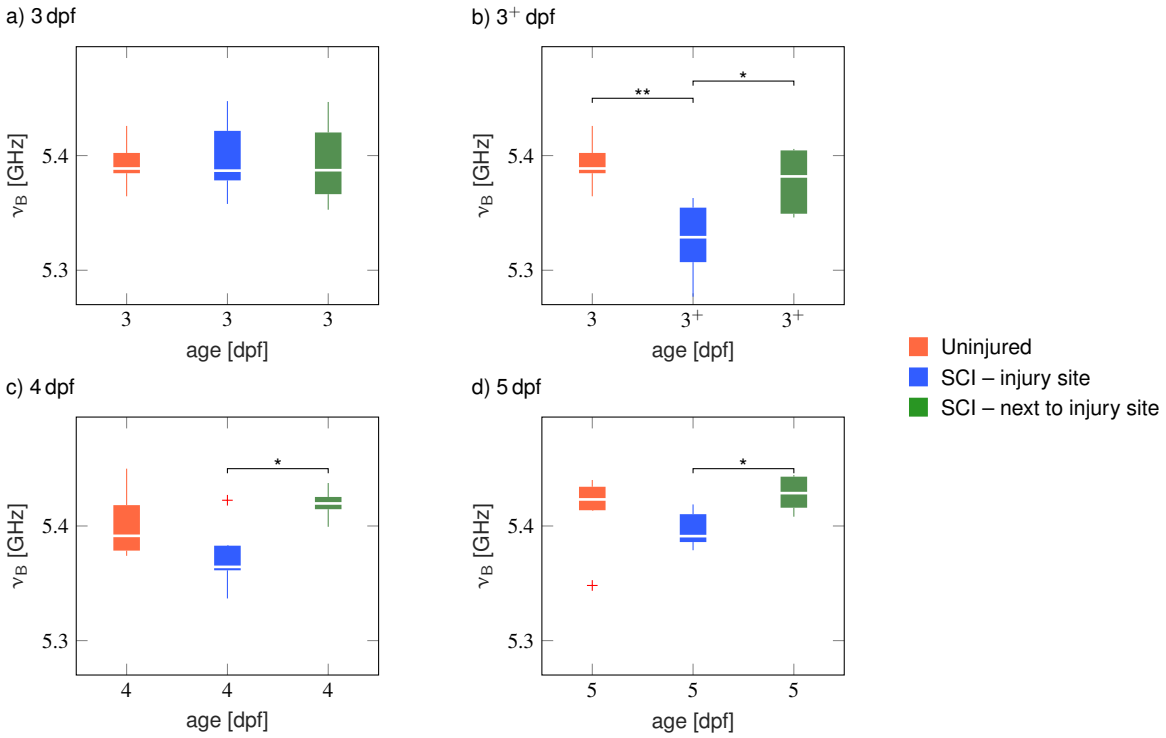

Supplementary Figure 4: Comparison of differently treated tissue regions at the same timepoints. a) – d) Box plots of the average Brillouin shifts of the respective areas in individual fish. The boxes indicate the interquartile ranges (IQR), the whiskers extend to the most extreme data still within 1.5 IQR of the respective quartile (Tukey boxplot) and the medians are depicted as white lines. Outliers are indicated as red crosses. b) $p_{■,■} = 0.004$, $p_{■,■} = 0.023$ c) $p_{■,■} = 0.011$ d) $p_{■,■} = 0.015$. $^{*}p < 0.05$ and $^{**}p < 0.01$.

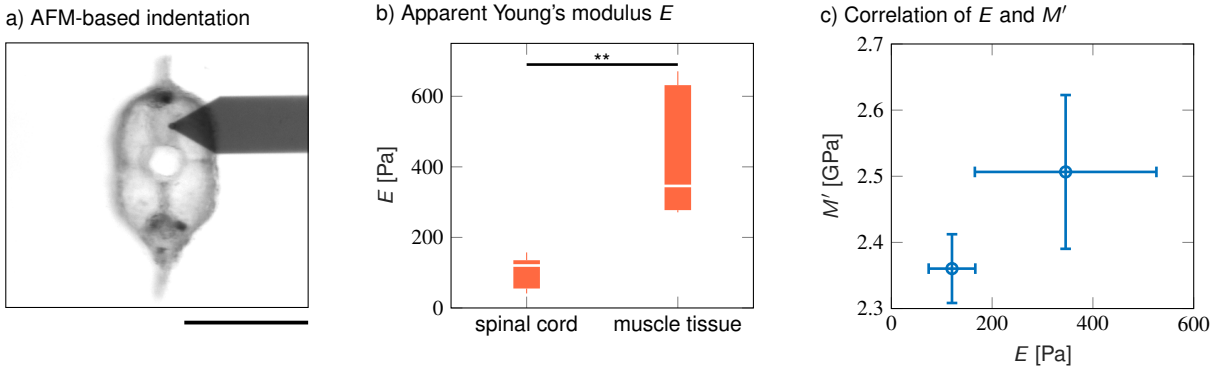

Supplementary Figure 5: AFM-based indentation measurements on acute, transverse zebrafish sections. a) Brightfield image of a representative sample section and a cantilever as observed during indentation measurements. Scale bar, 200 µm. b) Quantification of the apparent Young's modulus of the spinal cord (61 indentations) and the muscle tissue (74 indentations) for $N = 6$ zebrafish. The boxes indicate the interquartile ranges, the whiskers extend to the most extreme data still within 1.5 IQR of the respective quartile (Tukey boxplot) and the medians are depicted as white lines. $^{**}p < 0.01$. c) Correlation between the apparent Young's modulus E and the longitudinal modulus M' determined for zebrafish sections as shown in Fig. 7.

time points was not possible as the specimens turned opaque, which blocked proper light penetration. This decay process was reflected by measurement points that could not be analyzed (white pixels). After sacrificing and successive incubation in 4 % PFA overnight, zebrafish larvae exhibited greater Brillouin shifts in both muscle and spinal cord tissue (Supplementary Fig. 6c).

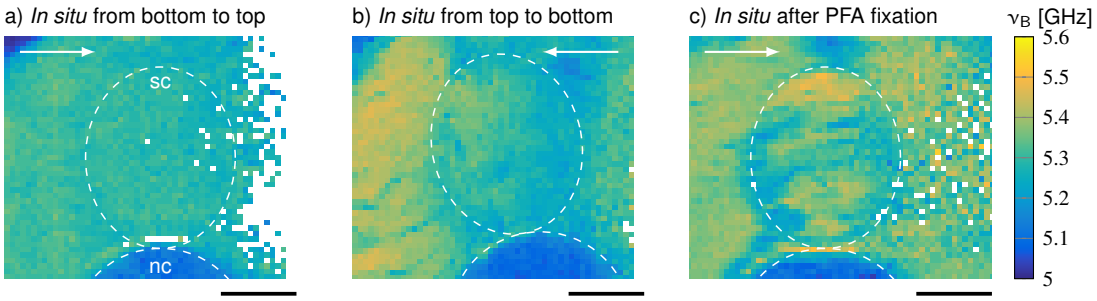

Supplementary Figure 6: Representative high-resolution Brillouin images of the perispinal area in acute zebrafish sections scanned from a) bottom to top and b) top to bottom as indicated by the white arrows. c) A dead zebrafish larva after 24 h incubation in 4 % PFA. The approximate positions of the spinal cords (sc) and the notochords (nc) are indicated by dashed lines. Scale bars, 25 µm.

Supplementary Note 4: Calculation of density from refractive index measurements

In order to calculate the longitudinal modulus M' from the measured Brillouin shift ν_B, the refractive index n and the absolute density ρ of the probed sample have to be known. The refractive index can be measured by quantitative phase imaging (QPI) or optical diffraction tomography (ODT). The absolute density can then be calculated from the refractive index.

Considering the sample under test as a two-substance mixture of a dry and a fluid fraction, one can express its absolute density ρ as

$$\rho = \frac{m_{\mathrm{dry}} + m_{\mathrm{fluid}}}{V} = \rho_{\mathrm{dry}} + \rho_{\mathrm{fluid}} \frac{V_{\mathrm{fluid}}}{V} = \rho_{\mathrm{dry}} + \rho_{\mathrm{fluid}} \cdot (1 - \rho_{\mathrm{dry}} \cdot \bar{\nu}_{\mathrm{dry}}) \quad [1]$$

with the mass m_{dry}, the mass density $\rho_{\mathrm{dry}} = \frac{m_{\mathrm{dry}}}{V}$, the partial specific volume $\bar{\nu}_{\mathrm{dry}} = \frac{V_{\mathrm{dry}}}{m_{\mathrm{dry}}}$ and the volume V_{dry} of the dry fraction; the mass m_{fluid}, the absolute density $\rho_{\mathrm{fluid}} = \frac{m_{\mathrm{fluid}}}{V_{\mathrm{fluid}}}$ and the volume V_{fluid} of the fluid fraction and the overall volume $V = V_{\mathrm{dry}} + V_{\mathrm{fluid}}$. The mass density of the dry fraction is given by (1–5)

$$\rho_{\mathrm{dry}} = \frac{n - n_{\mathrm{fluid}}}{\alpha} \quad [2]$$

with the measured refractive index n of the sample, the refractive index n_{fluid} of the fluid and the refraction increment $\alpha = 0.18\,\mathrm{ml/g}$ (3, 6). Hence, the absolute density can be calculated from the refractive index n, if the refraction increment, the refractive index of the fluid, the absolute density of the fluid and the absolute density of the dry fraction are known/constant. In case of $\rho_{\mathrm{dry}} \ll \frac{1}{\bar{\nu}_{\mathrm{dry}}}$ this can be approximated to

$$\rho \approx \frac{n - n_{\mathrm{fluid}}}{\alpha} + \rho_{\mathrm{fluid}}. \quad [3]$$

The partial specific volume for proteins is approximately $0.73\,\mathrm{ml/g}$(7). Hence, using the above approximation leads to an overestimation of the density by less than 4 % taking into account the variations of the refractive index measured in zebrafish larvae. We believe this error to be acceptable here. In conclusion, the longitudinal modulus then only depends on the Brillouin shift and the refractive index of the sample.

Supplementary Note 5: Relation between Brillouin signals and mechanical properties for hydrogels and glycerol-water mixtures

By taking into account the refractive indices and densities (see Supplementary Note 4) of polyacrylamide hydrogels of varying stiffness, the Brillouin shift can be used to calculate the longitudinal modulus M' of these gels. The longitudinal modulus correlates with the Young's modulus E, determined by AFM indentation measurements, following a log-log linear relationship (Supplementary Fig. 7a), confirming previous findings shown in (8). Likewise, the Brillouin peak linewidth can be converted into viscosity η_{B}. Using a falling ball viscometer, we determined the viscosity η_{FBV} of glycerol-water mixtures and found a linear correlation with the viscosities calculated from the Brillouin signals (Supplementary Fig. 7b). The viscosity η_{B} shows higher values than η_{FBV}, because the measured linewidth Δ_{B} is a convolution of the material's linewidth and the intrinsic spectrometer linewidth.

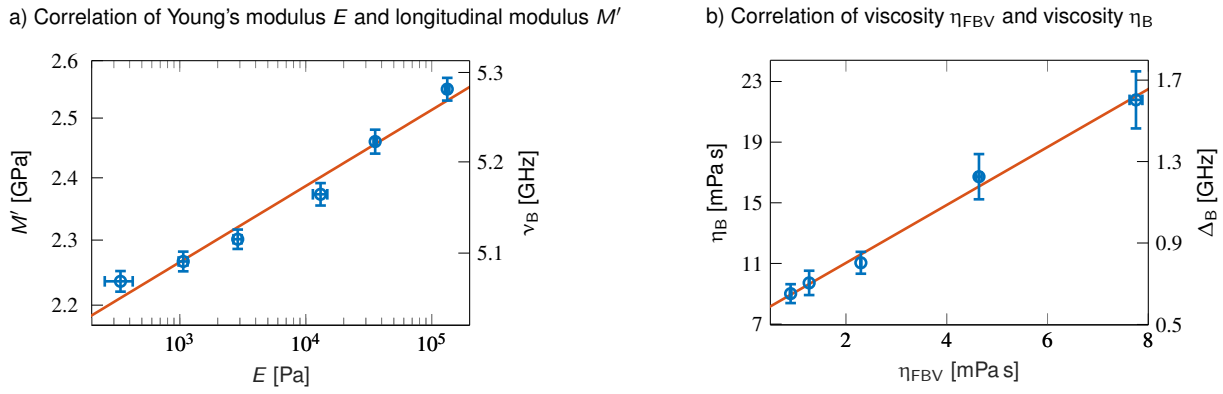

Supplementary Figure 7: a) The relation between the longitudinal modulus M' measured with Brillouin microscopy and the apparent Young's modulus E measured with indentation-type atomic force microscopy for polyacrylamide hydrogels shows a log-log linear relationship $\log(M') = a\log(E) + b$ with $a = 0.023$ and $b = 9.287$ (coefficient of determination $R^2 = 0.97$). b) The viscosity η_B calculated from the linewidth Δ_B of the Brillouin peak shows a linear dependence on the viscosity η_{FBV} measured with a falling ball viscosimeter (FBV) for glycerol-water mixtures with different mixture fractions ($R^2 > 0.99$).

SUPPLEMENTARY METHODS

AFM-based indentation measurements of zebrafish sections and PAA gels

Indentation measurements on transverse zebrafish sections were performed with the CellHesion200 (JPK Instruments) and the upright Axio Zoom.V16 stereo microscope using a PlanApo Z 0.5x objective (Carl Zeiss Microscopy). Polystyrene beads ($d = 10\,\mu m$, Microparticles GmbH) glued to tipless silicon cantilevers (Arrow-TL1, NanoWorld) served as indenters. Prior to each measurement, the sensitivities of the cantilevers were determined by obtaining force-distance curves on tissue culture plastic (TCP) in PBS. The spring constants of the cantilevers were determined with the thermal noise method (9) and only cantilevers with spring constants between $0.015\,N/m$ and $0.030\,N/m$ were used. Indentations commenced by manually positioning the indenter above targeted muscle and spinal cord areas and recording force-distance curves using an indentation force of $4\,nN$ and an indentation speed of $10\,\mu m/s$. All indentation measurements of zebrafish sections took place at $20\,^{\circ}C$.
The mechanical properties of the PAA gels were measured using an a NanoWizard 4 (JPK instruments, Germany). PNP-TR-TL (Nanoworld) cantilevers with a spring constant of $75\,mN/m$ were used after attaching $5\,\mu m$ polystyrene beads to their tip. Calibration was performed as described for zebrafish sections. Every gel was indented in 10 different areas, each area consisted of 16 equally separated points on a $50\,\mu m \times 50\,\mu m$ grid. The indentation speed was set to $5\,\mu m/s$ and the force applied ranged between $1.5\,nN$ to $15\,nN$. All indentation measurements on gels were conducted at room temperature.
Individual indentations yield force-distance curves. These were analyzed using the JPK data processing software (JPK Instruments) in which the indentation segments of the approach curves are fitted with the Hertz model modified for a spherical indenter:

$$F = \frac{E}{1-\nu^2} \times \left(\frac{R^2+r^2}{2} \ln \frac{r+R}{r-R} - Rr \right) \quad [4]$$

with

$$\delta = \frac{R}{2} \ln \left(\frac{r+R}{r-R} \right), \quad [5]$$

where F denotes the indentation force, δ the indentation depth, r the indenter radius and R the radius of the circular contact area between indenter and sample (10–12). The Poisson's ratio ν was set to 0.5 for all analyses. The Young's modulus E is used as the fitting parameter and serves as a measure of elastic stiffness.

Preparation of polyacrylamide gels

Polyacrylamide gels were prepared as described in (13). Briefly, $13\,mm$ diameter glass coverslips were first washed with $0.1\,N$ NaOH, dried and then soaked in a solution of $30\,ml$ chloroform (Sigma-Aldrich, Germany), $30\,\mu l$ Triethylamine (Sigma-Aldrich, Germany) and $30\,\mu l$ Allylthrichlorosilane (Sigma-Aldrich, Germany). Afterwards, the glasses were washed, dried and an amount of $300\,\mu l$ of 0.5 % Glutaraldehyde was added to each of them. The glasses were incubated for 45 minutes before they were washed and dried. To obtain a wide range of PAA elasticities, premixes of phosphate buffered saline (PBS), 40 %

acrylamide (Sigma-Aldrich, Germany) and 2 % N,N'-Methylenebisacrylamide (Bis-acrylamide) (Sigma-Aldrich, Germany) were prepared according to table 1 (13).

Gel no.	% Acrylamide	% Bis-acrylamide
1	5	0.04
2	5	0.07
3	7.5	0.06
4	7.5	0.2
5	12	0.2
6	18	0.4

Supplementary Table 1: Composition of the different PAA gels.

To initiate the polymerization, 1 % of ammonium persulfate (Sigma-Aldrich, Germany) and 0.3 % of N,N,N',N'-Tetramethylethylenediamine (TEMED) (Sigma-Aldrich, Germany) were added to the premixed solutions. The gel mixtures were immediately placed on the glass coverslips, polymerized for 30 minutes and then placed in PBS solution. The gels were incubated overnight in 4 °C to allow maximal gel swelling before measuring the mechanical properties. Similarly, a set of PAA gels without a glass coverslip was prepared to allow measurements of the refractive index. The refractive index of the gels was measured with an Abbe refractometer (2WAJ, Arcarda) one day after preparation, the density was calculated from the refractive index according to Supplementary Note 4.

Measurement of the viscosity of glycerol-water-mixtures with a falling ball viscometer

The viscosity η_{FBV} of glycerol-water mixtures with different mixture fractions was measured with a falling ball viscometer (Haake falling ball viscometer Typ C, Thermo-Scientific) according to the manufacturer's instructions. The mixtures contained 0 %, 10 %, 25 %, 40 % and 50 % (v/v) glycerol. The refractive index of the mixtures was measured with an Abbe refractometer (2WAJ, Arcarda), the density was measured by weighing a volume of 50 ml of each mixture.

REFERENCES

1. Barer, R., 1952. Interference Microscopy and Mass Determination. *Nature* 169:366–367. http://dx.doi.org/10.1038/169366b0.

2. Davies, H. G., and M. H. F. Wilkins, 1952. Interference Microscopy and Mass Determination. *Nature* 169:541–541. http://dx.doi.org/10.1038/169541a0.

3. Zangle, T. A., and M. A. Teitell, 2014. Live-cell mass profiling: an emerging approach in quantitative biophysics. *Nat Meth* 11:1221–1228. http://dx.doi.org/10.1038/nmeth.3175.

4. Popescu, G., Y. Park, N. Lue, C. Best-Popescu, L. Deflores, R. R. Dasari, M. S. Feld, and K. Badizadegan, 2008. Optical imaging of cell mass and growth dynamics. *American Journal of Physiology - Cell Physiology* 295:C538–C544. http://www.ncbi.nlm.nih.gov/pmc/articles/PMC2518415/.

5. Schürmann, M., J. Scholze, P. Müller, J. Guck, and C. J. Chan, 2016. Cell nuclei have lower refractive index and mass density than cytoplasm. *Journal of Biophotonics* 9:1068–1076. http://dx.doi.org/10.1002/jbio.201500273.

6. Barer, R., and S. Joseph, 1954. Refractometry of Living Cells. *Journal of Cell Science* s3-95:399–423. http://jcs.biologists.org/content/s3-95/32/399.

7. Harpaz, Y., M. Gerstein, and C. Chothia, 1994. Volume changes on protein folding. *Structure* 2:641–649. http://dx.doi.org/10.1016/S0969-2126(00)00065-4.

8. Scarcelli, G., P. Kim, and S. Yun, 2011. *In vivo* Measurement of Age-Related Stiffening in the Crystalline Lens by Brillouin Optical Microscopy. *Biophysical Journal* 101:1539 – 1545. http://www.sciencedirect.com/science/article/pii/S0006349511009507.

9. Hutter, J. L., and J. Bechhoefer, 1993. Calibration of atomic-force microscope tips. *Review of Scientific Instruments* 64:1868–1873. https://doi.org/10.1063/1.1143970.

10. Hertz, H., 1881. Ueber die Berührung fester elastischer Körper. *Journal für die reine und angewandte Mathematik* 92.

11. Sneddon, I., 1965. The relation between load and penetration in the axisymmetric Boussinesq problem for a punch of arbitrary profile. *International Journal of Engineering Science* 3:47–57.

12. JPK Instruments. Determining the elastic modulus of biological samples using atomic force microscopy. Technical report.

13. Moshayedi, P., L. D. Costa, A. Christ, S. P. Lacour, J. Fawcett, J. Guck, and K. Franze, 2010. Mechanosensitivity of astrocytes on optimized polyacrylamide gels analyzed by quantitative morphometry. *J. Phys. Condens. Matter* 22:194114.